Assessment of weak compressibility in actuator line simulations of wind turbine wakes

Assessment of weak compressibility in actuator line simulations of wind turbine wakes

Henrik Asmuth[1]**, Christian F. Janßen**[2]**, Hugo Olivares-Espinosa**[1]**,
Karl Nilsson**[1]**, Stefan Ivanell**[1]

[1] Uppsala University, Wind Energy Section, Campus Gotland, 621 57 Visby, Sweden
[2] Hamburg University of Technology, Institute of Fluid Dynamics and Ship Theory M-8, Am Schwarzenberg-Campus 4 (C), 21073 Hamburg

E-mail: `henrik.asmuth@geo.uu.se`

Abstract. The trend of increasing rotor diameters and tip-speeds has brought about concerns of non-negligible compressibility effects in wind turbine aerodynamics. The investigation of such effects on wakes is particularly difficult when using actuator line models (ALM). This is because crucial regions of the flow, i.e. the direct vicinity of the blade, are not simulated but represented by body forces. To separately assess the impact of compressibility on the wake and the ALM itself, we conduct large-eddy simulations (LES) where the forces of the ALM are prescribed and based on the local sampled velocity (standard procedure), respectively. The LES are based on the weakly-compressible Lattice Boltzmann Method (LBM). Further to the comparison of (near-)incompressible to compressible simulations we investigate cases with artificially increased compressibility. This is commonly done in weakly-compressible approaches to reduce the computational demand. The investigation with prescribed forces shows that compressibility effects in the wake flow are negligible. Small differences in the wake velocity (of max. 1%) are found to be related to local compressibility effects in the direct vicinity of the ALM. Most significantly, compressibility is found to affect the sampled velocity and thereby accuracy of the ALM.

1. Introduction

Traditionally, the numerical modeling of wind turbine and farm aerodynamics is performed in incompressible frameworks [1]. This choice is generally well in line with the underlying incompressibility assumption ($\mathrm{Ma} < 0.3$) as tip speeds usually lie below $100\,\mathrm{m\,s^{-1}}$ [2]. Recently, however, the occurrence of local Mach numbers beyond this incompressible regime has become more likely due ever increasing turbine sizes and rotor radii approaching the $100\,\mathrm{m}$ mark. Several studies therefore investigated compressibility effects on airfoil properties [3, 4]. These show that there are non-negligible changes in the lift and drag that should be taken into account. Sørensen et al. [4] also showed that common compressibility corrections to incompressible airfoil data such as the Prantl-Glauert correction [5] are in reasonable agreement with the compressible data. Based on such compressibility-corrected airfoil properties Yan and Archer [6] investigated the effects of compressibility on the overall power and thrust coefficient C_P and C_T, respectively, of an entire turbine. Using a standard blade element momentum (BEM) approach they found that noticeable effects on C_P and C_T only occur at wind speeds u_0 and tip speed ratios (TSR) that are beyond typical operating conditions ($u_0 > 15\mathrm{m\,s^{-1}}$, TSR > 12). In any case, the occurrence

of high local Mach numbers in the flow past wind turbines mostly results from the rotation of the blade. Therefore, Wood [7] assumed that compressibility effects are confined to the flow over the blade. Flow fields obtained from geometrically resolved simulations of full-scale rotors corroborate this assumption. They show that velocities approaching the compressible regime are limited to the boundary layer of the airfoil [8, 9]. It therefore appears that compressibility only plays an indirect role when it comes to the wake of the turbine. To be clear, compressibility-related changes in C_T and C_P can obviously alter the wake characteristics. Nevertheless, the wake flow itself remains in the weakly compressible regime where the effect of density fluctuations on the solenoidal (incompressible) velocity components is negligible.

These considerations become particularly interesting when the turbine is represented by the actuator line model (ALM). The ALM, commonly used in large-eddy simulations (LES) of wind turbines [1], applies velocity-dependent lift and drag forces of discrete airfoil sections as body forces in the computational domain [10]. The aforementioned regions prone to non-negligible compressibility are thus not explicitly captured when using the ALM. Yan and Archer [6] also investigated compressibility effects when using the ALM. The authors compared turbine performance and wake properties obtained from both compressible and incompressible LES while using the same uncorrected (incompressible) airfoil data. Even for cases with presumably low compressibility effects on the airfoil properties ($u_0 = 7.88\,\mathrm{m\,s^{-1}}$, TSR=8) notably smaller velocity deficits and turbulent kinetic energies were obtained in the compressible framework. The authors argued that these differences are related to an upstream reduction of kinetic energy due to compression. However, this interpretation is arguably bold in light of turbulent Mach numbers $M_t = \sqrt{k}/c_s$ (where k is the turbulent kinetic energy and c_s the speed of sound) being reported in the order $\mathcal{O}(10^{-3})$. Both theory and fundamental investigations of compressible turbulence suggest that such interactions of dilatational and solenoidal components are typically weak in this low-Mach number quasi-isentropic regime ($M_t < 0.1 .. 0.3$) [11, 12, 13, 14].

In addition to purely physical aspects, compressibility does become relevant from a numerical stand point in weakly compressible formulations. Weakly compressible schemes solve the compressible Navier-Stokes equations but lack an explicit formulation of the total energy. The temperature of the simulated system is thus inherently constant. The effects of temperature fluctuations are consequently not captured thereby limiting the use to the quasi-isentropic regime and compressible phenomena such as acoustics [12]. When applied to incompressible flow problems, the occurring compressibility effects are often seen as a mere numerical artefact. As a matter of fact though, in practice simulations are often run with lower c_s than found in the actual flow problem. Such a choice is motivated by lower computational costs as c_s is inversely proportional to the time step Δt [15].

In this study we are specifically concerned with the Lattice Boltzmann Method (LBM). Due to its excellent computational efficiency the LBM has shown to be a promising alternative to common CFD approaches [16], also in the field of wind energy [17, 18, 19, 20]. The LBM in its classical form is a weakly compressible formulation. The motivation for an assessment of weak compressibility effects in ALM simulation of wind turbines is thus twofold. Firstly, recent discussions of compressibility effects on wakes [6] appear to require additional considerations due to the aspects outlined above. Among others, Meyer-Forsting et al. [21] showed that the velocity induced by the ALM itself can have severe impacts on the correct computation of the body forces. Moreover, in Asmuth et al. [19] it was shown that this inherent problem of the ALM not only depends on the width of the model's smearing kernel ϵ but also the Mach number. We therefore argue that it is crucial to separate the investigation of compressibility effects between the ALM and the wake. To this end, we perform ALM simulations with the LBM at different c_s while prescribing the body forces along the actuator line. This permits to avoid potential differences that could arise from the interaction of the ALM with the flow field. For instance, those caused by the changes in angle of attack due to variations in the induced velocity. The

latter was shown to be one of the most sensitive aspects of the ALM when it comes to the correct representation of the body forces [21]. Most importantly, this aspect relates to a model-specific issue rather than a correct representation of the interaction of the blade with the surrounding fluid, be it compressible or incompressible. In a second suite of simulations we use the standard ALM approach as in [6]. Here, we examine what factors influence the forces along the blade at different compressibilities and how this again affects the wake characteristics.

The second motivation for this study is more specific to wake simulations using the LBM or other weakly compressible approaches as in [22, 23]. As outlined above, c_s is often chosen lower than physical. If compressibility effects were to have non-negligible effects on wakes of modern wind turbines it is crucial to assess how these effects evolve when artificially increasing the compressibility in a weakly compressible framework. The aforementioned test series therefore comprise cases with the physically correct speed of sound as well as larger (less compressible) and lower values (more compressible).

2. The Lattice Boltzmann Method
As opposed to classical Navier-Stokes-based CFD approaches the LBM solves the kinetic Boltzmann equation. For the sake of brevity we can only give a brief introduction to the underlying numerical concepts. For a more comprehensive overview we refer to the work by Krüger et al. [24].

2.1. Governing Equation
The kinetic Boltzmann equation describes the dynamics of so called particle distribution functions f. These characterise the probability to encounter a particle (mass) density of velocity $\boldsymbol{\xi}$ at time t at location $\boldsymbol{x}$. Solving the kinetic Boltzmann equation therefore requires a discretisation in both physical and velocity space. Using a finite-difference approach in space and time and a set of discrete velocities (referred to as velocity lattice) we obtain the lattice Boltzmann equation (LBE)

$$f_{ijk}(t + \Delta t, \boldsymbol{x} + \Delta t\, \boldsymbol{e}_{ijk}) - f_{ijk}(t, \boldsymbol{x}) = \Omega_{ijk} \tag{1}$$

where $\boldsymbol{e}_{ijk} = i\boldsymbol{e}_x + j\boldsymbol{e}_y + k\boldsymbol{e}_z$ is the referring velocity vector of each discrete lattice direction. The collision operator Ω_{ijk} models the redistribution of f through particle collisions, described by a relaxation towards a Maxwellian equilibrium. Following dimensional analysis we obtain a macroscopic description of the fluid by means of the raw velocity moments of f

$$m_{\alpha\beta\gamma} = \sum_{ijk} i^\alpha j^\beta k^\gamma\, f_{ijk} \tag{2}$$

where α, β and γ denote the order of the moment in the referring lattice direction. Using eq. (2), the mass density ρ is then obtained from the zeroth-order moment m_{000}. Analogously, the momentum in x, y and z is given by the first-order moment in the referring coordinate direction m_{100}, m_{010} and m_{001}, respectively. In the classical BGK (Bhatnagar-Gross-Kroog [25]) collision model the particle distribution functions are directly relaxed towards the equilibrium using a single constant relaxation rate ω. Due to poor numerical stability numerous alternative collision models have been suggested. A comprehensive review thereupon can be found in [26]. In this work we apply the cumulant collision model (CLBM) introduced by Geier et al. [27]. As opposed to the BGK or moment-based multiple relaxation time models (MRT) as, for instance, [28], the CLBM relaxes cumulants of the PDFs, i.e. independent observable quantities. Substantial advantages of the CLBM are a maximisation of Galilean invariance and the elimination of spurious couplings between observable quantities. As a result, the CLBM provides a drastic reduction of numerical errors and improved numerical stability especially for high-Reynolds number flows [27, 29].

2.2. Compressibility in the Lattice Boltzmann Method

A Chapman-Enskog [24] or Taylor expansion [30] of the LBE reveals that it recovers the compressible Navier-Stokes equations with a corresponding isothermal equation of state $p = \rho c_s^2$. The LBM thus inherently captures weakly compressible phenomena as found in low Mach number flows. Among others, it is therefore commonly applied in the field of aeroacoustics. See, for instance [31, 32].

From a physical point of view, the isothermal assumption of the LBM prohibits the simulation of flows beyond the weakly compressible regime. In addition, the use of classical collision operators like the BGK or MRT is numerically limited to low Mach numbers. The latter relates to a velocity-dependent error $\mathcal{O}(u^3)$ in the recovery of the stress tensor. As the velocity u on the lattice level scales with the Mach number this viscosity error itself effectively scales with Ma^2 [33]. Low Mach numbers are therefore required in order to keep the cubic defect in reasonable bounds. Or, framing it inversely, changes in compressibility can imply changes in the numerical diffusivity. The CLBM, however, corrects for this defect as well as other violations of Galilean invariance. Also, the use of parametrised collision rates [29] further reduces Ma-dependent errors in the viscosity. Accordingly, the CLBM appears as a suitable method to investigate compressible phenomena in wind turbine wakes in a range of low Mach numbers.

2.3. The Actuator Line Model

The utilised ALM closely follows the standard procedures presented in [10] and others. The forces at each blade element of the actuator line are determined using the respective relative velocity u_{rel}, with

$$u_{rel} = \sqrt{u_n^2 + (\Omega\, r - u_\theta)^2} \quad , \tag{3}$$

where u_n is the blade-normal (streamwise) velocity, u_θ the tangential velocity, Ω the rotational velocity of the turbine and r the radial position of the blade element. The local blade forces per unit length are given by

$$\boldsymbol{F} = 0.5\, \rho\, u_{rel}^2\, c\, (C_L(\alpha)\, \boldsymbol{e}_L + C_D(\alpha)\, \boldsymbol{e}_D) \quad , \tag{4}$$

with ρ being the fluid density and c the chord length. The lift and drag coefficients C_L and C_D, respectively, are interpolated from tabulated airfoil data as functions of the local angle of attack α. The blade forces are smeared in space using a three-dimensional Gaussian convolution kernel with characteristic smearing width ϵ. The resulting body force per control volume is finally applied in the CLBM collision operator. Further details upon the latter can be found in the original work by Geier et al. [27].

3. Numerical Framework

3.1. The Lattice Boltzmann Solver ELBE

The simulations are performed with the GPU-based Efficient Lattice Boltzmann Environment ELBE[1] [34] mainly developed at Hamburg University of Technology (TUHH). The CLBM implementation in ELBE was recently validated by Gehrke et al. [35, 36] by means of several fundamental test cases. Further applications include ALM simulations as presented in [19, 20].

3.2. Case set-up

The presented investigation is based on simulations of the NREL 5MW reference turbine [37] in a sheared turbulent inflow. The simulated turbine is situated in a rectangular domain of 20 rotor diameters D in the stream-wise direction x and $6\,D$ in the lateral direction y and vertical direction z, respectively. The uniform grid spacing measures $\Delta x = D/32$. The turbine is located

---

[1] https://www.tuhh.de/elbe

$3\,D$ downstream of the inlet. Furthermore, we define the coordinate origin such that the turbine hub refers to $\boldsymbol{x} = \{0, 0, z_{hub} = 0.79\,D\}$.

The velocity at the inlet is prescribed by a logarithmic profile $u(z) = u^*/\kappa \ln(z/z_0)$ that is perturbed with synthetic Mann turbulence [38]. At the top we prescribe a geostrophic wind based on the velocity profile. The lateral direction is periodic and an extrapolation boundary condition is applied at the outlet. At the bottom we also apply a velocity boundary condition with $u_{BC} = u(z = \Delta x)$. Mind, that wall modelling in the LBM is still at an early stage when compared to classical LES [39, 40]. It is therefore not considered in this study. As for the CLBM scheme, we apply a limiter $\lambda = 0.01$ to the relaxation of the third-order cumulants as suggested in [29]. Furthermore, the CLBM is applied without explicit turbulence model, in line with various other studies [15, 20, 36].

The inlet velocity is chosen such that the turbine operates at rated power, i.e. $u_0 = 11.4\mathrm{m\,s^{-1}}$ ($u^* = 0.495\mathrm{m\,s^{-1}}$, $z_0 = 0.01\mathrm{m}$). The imposed Mann turbulence refers to a turbulence intensity of $\mathrm{Ti}_0 = 2.8\%$. The rotational speed of the turbine is fixed based on the optimal tip-speed ratio TSR = 7.55. This point of operation implies the highest possible local Mach numbers at the blades excluding above-rated conditions. All simulations are run for a total of 18 domain flow-through times T_{ft} with respect to u_0. Statistics are gathered after $6\,T_{ft}$. In each test series we investigate four different speeds of sound. All cases will be referred to with a corresponding Mach number with respect to u_0. The lowest Mach number $\mathrm{Ma}_{0.5pc} = 0.017$ corresponds to twice the actual speed of sound with $c_s = 680\mathrm{m\,s^{-1}}$. This case shall serve as a near-incompressible (NI) reference as compressibility is indeed negligible as shown in section 4.1. Accordingly, Ma_{pc} corresponds to the physically correct (PC) Mach number (Mach-matched). Ma_{2pc} and Ma_{4pc} refer to a half and a quarter the physically correct c_s, respectively (more compressible). Furthermore, note, that Ma_{2pc} and Ma_{4pc} are commonly found in the literature when simulating supposedly incompressible flow problems with the LBM. All cases are run with smearing widths of $\epsilon = 1\,\Delta x$ and $\epsilon = 2\,\Delta x$, respectively in order to assess the impact of the regularisation kernel.

For the sake of consistency it should also be mentioned that all cases are run in double-precision floating-point format in order to accurately represent the non-dimensional viscosity in the LBM scheme at all Ma. In single-precision, which is commonly used in GPU-based LBM solvers, the viscosity with $\mathrm{Ma}_{0.5pc}$ would be numerically indistinguishable from zero. For a further discussion of this topic the interested reader is referred to Lenz et al. [15].

4. Results and Discussion

4.1. Prescribed Rotor Loads

In the first test series we decouple the ALM from the surrounding fluid. Therefore, the local velocity in eq. (4) is prescribed by the inlet velocity profile, i.e. $u_n = u(z)$ and $u_\theta = 0$, and not sampled from the flow field. In fig. 1 we compare the difference of each case with $\epsilon = 1\,\Delta x$ towards the reference $\mathrm{Ma}_{r,\mathrm{NI}}$ in the mean streamwise velocity $\Delta \bar{u}(x, z) = \bar{u}(x, z) - \bar{u}_{r,\mathrm{NI}}(x, z)$ as well as turbulence intensity $\Delta \mathrm{Ti}(x, z) = \mathrm{Ti}(x, z) - \mathrm{Ti}_{r,\mathrm{NI}}(x, z)$ normalised by u_0 and Ti_0, respectively. The most distinct differences in the velocity can be found in the the near-wake. Here, the velocity deficit in the upper shear layer is lower than in the reference while the opposite holds for the lower shear layer. This characteristic gets more pronounced the higher the Mach number with a maximum difference of about 2.5% for Ma_{4pc}. Further downstream a clear trend can not be observed as differences are more scattered in space. The turbulence intensity in the near-wake decreases the higher Ma. In the far-wake differences are again rather scattered except for Ma_{4pc}. The latter case shows notably higher Ti in the entrainment zone as the wake recovers.

For a better quantification of the differences we compute the spatial mean of the magnitude of the difference in the velocity and turbulence intensity $\langle |\Delta \bar{u}| \rangle$ and $\langle |\Delta \mathrm{Ti}| \rangle$ within cross-sectional planes of $-D \leq y \leq D$, $z \leq 2D$ at different positions x, shown in fig. 2. As an additional reference we provide the the differences found in cases without turbine. Mind, that results of the
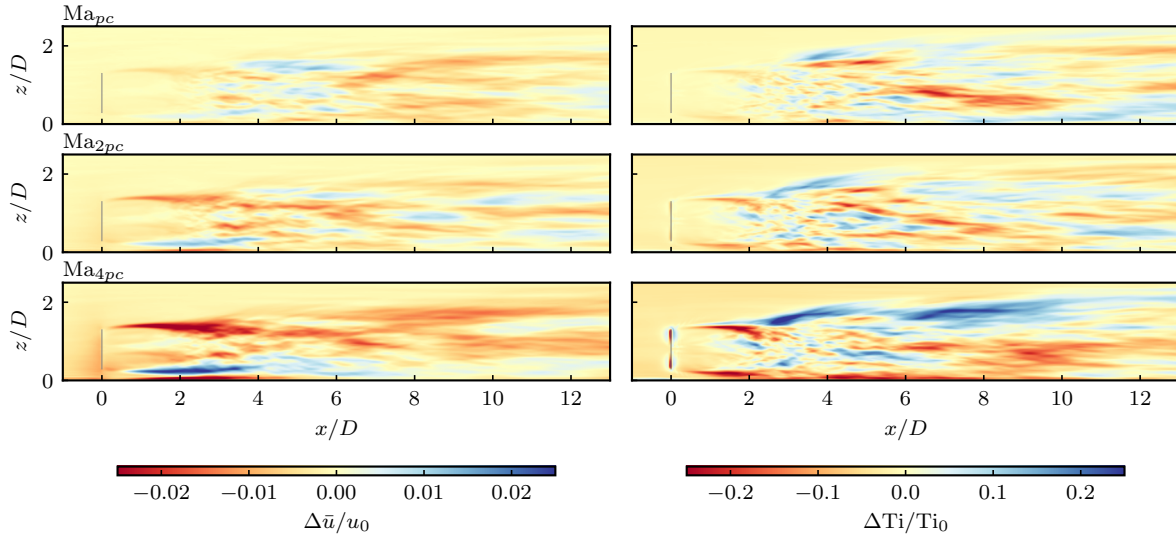
Figure 1: Contour plots of the normalised difference in mean streamwise velocity $\Delta u/u_0$ (left) and turbulence intensity $\Delta \mathrm{Ti}/\mathrm{Ti}_0$ (right) in vertical planes at $y = 0$ with $\epsilon = 1\,\Delta x$. Grey line inidcating the rotor plane.
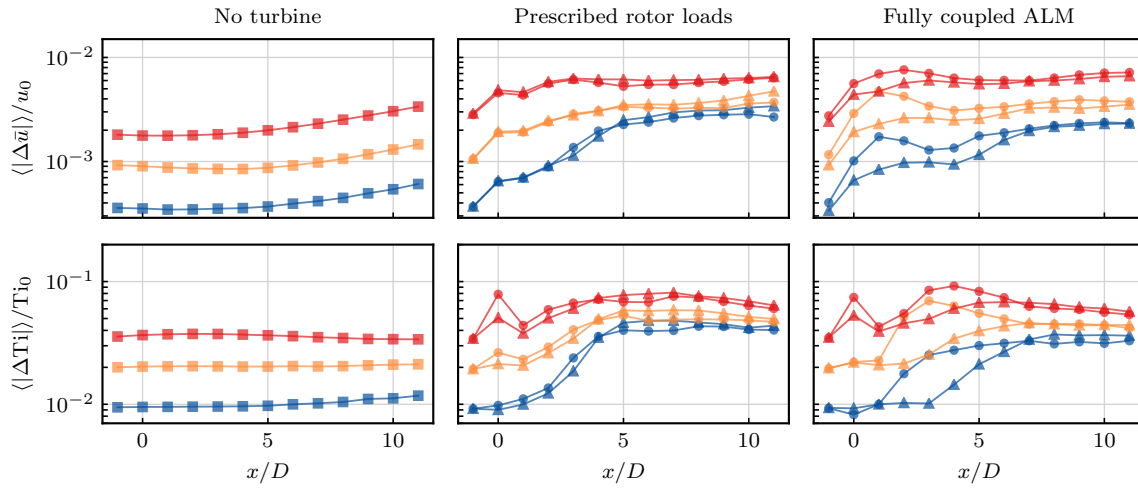

Figure 2: Spatial mean of the absolute error of $\bar{u}$ and Ti across cross-sectional planes at different downstream positions. No turbine (Ma_{pc}:■, Ma_{2pc}:■, Ma_{4pc}:■), $\epsilon = 1\,\Delta x$ (●,●,●), $\epsilon = 2\,\Delta x$ (▲,▲,▲).

fully coupled ALM cases will be discussed in section 4.2. First of all, the impact of compressibility on the ambient flow (no turbine) is found to be small. The difference in $\bar{u}$ between the PC and the NI case amounts to less than 0.1% in all investigated cross sections. With higher Ma the differences increase, yet remain below 0.5% in the entire domain. As for the Ti the differences are about one order of magnitude higher with a maximum of about 4% for the highest Ma. The presence of the turbine increases Ma-related differences when compared to the ambient flow. Particularly, the differences grow throughout the near-wake but remain rather constant in the far-wake. Generally, it can be seen that the magnitude of the deviations is close to the one in
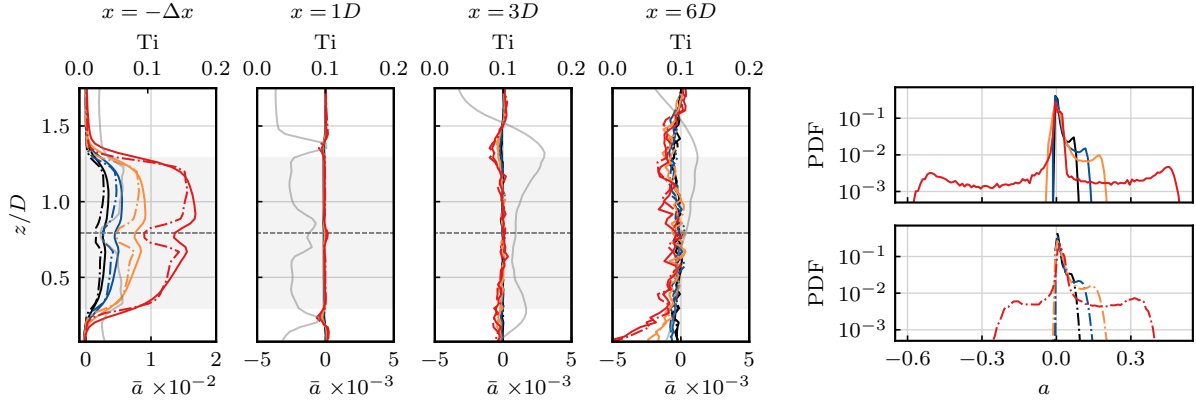
Figure 3: Comparison of the relative dilatation. *Left*: vertical profiles of the mean relative dilatation $\bar{a}$ at different positions downstream. $\epsilon = 1\,\Delta x$: $\mathrm{Ma}_{0.5pc}$ (—), Ma_{pc} (—), Ma_{2pc} (—), Ma_{4pc} (—). $\epsilon = 2\,\Delta x$ in corresponding dashed-dotted lines. Mind the different of scale on the abscissa at $x = -\Delta x$. Ti of Ma_{pc} (—) is given with respect to the upper abscissa. Dashed grey line marking z_{hub}. Rotor swept area shaded in light grey. *Right*: PDF of a at $\boldsymbol{x} = (-\Delta x, 0, z_{hub} + R)$.

the ambient flow up until the rotor plane. Thus, turbine-induced compression/expansion mostly seems to affect the flow field downstream. The effect of the smearing width ϵ on the velocity is found to be mostly negligible. A notable impact can only be observed in the Ti in the rotor plane which increases with Ma. The latter can be expected since smaller ϵ imply higher local pressure gradients which again lead to larger changes in density the higher Ma. Nevertheless, it is noticeable that ϵ only plays a minor role downstream of the rotor.

In order to characterise the occurring compressibility we evaluate the relative dilation

$$a = \frac{\partial u_i}{\partial x_i} \left(\frac{\partial u_n}{\partial x_m} \frac{\partial u_n}{\partial x_m} \right)^{-\frac{1}{2}}, \tag{5}$$

i.e. the velocity dilatation (divergence) normalised by the magnitude of the velocity gradient tensor. Algebraically, a is limited to the range $\{-\sqrt{3}, \sqrt{3}\}$. Negative values indicate compression (decrease in volume) while positive values indicate expansion (increase in volume) [41]. Statistical comparisons of a are depicted in fig. 3. Mind, that we choose to show $\bar{a}$ at $x = -\Delta x$ instead of the rotor plane since the latter corresponds to the zero-crossing of $\bar{a}$ in the stream-wise direction. Accordingly, we find almost the exact negative of this profile at $x = \Delta x$. In the wake departures from zero only occur in regions of high Ti. Yet, the magnitude thereof is consistently low. Even for the highest Ma maximal values are $\mathcal{O}(10^{-3})$ which can be considered negligible referring to fundamental studies of compressible turbulence [41, 42]. The latter is not surprising in the sense that local turbulent Mach numbers in Ma_{4pc} are $\mathcal{O}(10^{-2})$ and correspondingly lower in the other cases. Hence, the wake flow consistently corresponds to the weakly compressible regime where compressibility effects are negligible. The mean dilatation close to the ALM is considerably higher, yet still low in absolute terms. On the other hand, the probability density function (PDF) of a reveals that non-negligible dilatations do occur. This particularly stands out for Ma_{4pc} showing secondary peaks at relatively large positive and negative values. The spectra of a (not shown here for the sake of brevity) prove the obvious conjecture that these peaks originate from the blade passage. This also explains the lower magnitude of the secondary peaks with $\epsilon = 2\Delta x$. Moreover, it is noticeable that major changes
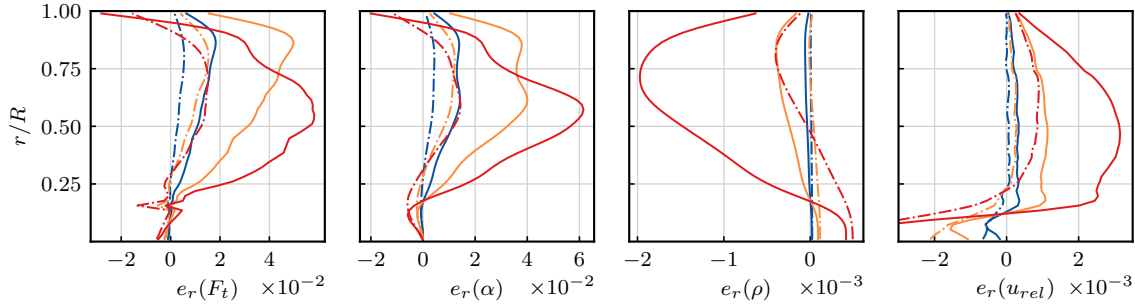
Figure 4: Relative difference e_r of the tangential force F_t, angle of attack α, mean density ρ and relative velocity u_{rel} (from left to right) with respect to the NI reference case along the actuator line with $\epsilon = 1\,\Delta x$ and $\epsilon = 2\,\Delta x$ using the same colors and lines as in fig. 3.

in the PDF due to ϵ only occur with Ma_{4pc}. Note, that the effect thereof was shown earlier in fig. 2 in terms of an increased $\langle|\Delta\mathrm{Ti}|\rangle$ in the rotor plane.

4.2. Fully Coupled ALM
The second test series investigates the standard fully coupled ALM as described in section 2.3. The L^1-norm given in fig. 2 shows that Ma-related changes in the velocity behave similarly with $\epsilon = 2\Delta x$ when compared to the cases with prescribed forces. The same accounts for the turbulence intensity. With $\epsilon = 1\Delta x$ differences in the rotor plane and near-wake increase notably. Also, deviations of Ti towards the reference show a significant increase in the near-wake region in comparison to $\epsilon = 2\Delta x$. The force distribution along the actuator line reveals that higher deviations in the flow field go along with corresponding changes in the forces. An estimate thereof can be obtained from the relative difference of the tangential force F_t towards the reference ($e_r(F_t) = F_t/F_{t,\mathrm{NI}} - 1$) depicted in fig. 4. Similar characteristics are found for the normal force F_n which is omitted here in the interest of brevity. Moreover, the sensitivity of the forces to compressibility is found to be larger the smaller ϵ.

From eq. (4) we can also identify possible terms causing changes in F_t and F_n. The influence of the flow field on the magnitude of u_{rel} is naturally small since it is dominated by $\Omega\,r$ which we set. Also, deviations of the mean density from the reference case only amount to a maximum of 0.2%, see fig. 4. Hence, we can identify the angle of attack as the main influencing factor on $e_r(F_t)$ based on both magnitude and correlation with $e_r(F_t)$. To be precise, the correlation coefficient of the two errors $R_{F_t,\alpha} > 0.95$ for all cases. Moreover, supplementary simulations in uniform inflow (not shown here for the sake of brevity and, similar to the findings presented in [19]) reveal that large $e_r(F_t)$ also imply large deviations from BEM results.

Force deviations of the ALM from BEM or lifting line theory have been widely discussed in the literature [43, 21, 44]. Typically, these are found near the root and tip of the blade. Meyer Forsting et al. [21] discussed that such deviations mostly relate to changes in the angle of attack due to the velocity induction of the trailing vortices. Here we show that an increasing compressibility as well as decreasing smearing width introduce an additional error in α. This, however, is not concentrated at the root and tip as shown in fig. 4. It therefore appears that low ϵ and high Ma also affect the bound vortex of the actuator line and thereby the sampled velocity along the line.

5. Conclusion
The present work investigates several aspects of compressibility in ALM simulations of wind turbine wakes in weakly compressible frameworks. Firstly, the analysis of cases with prescribed

rotor forces showed that non-negligible compressibility effects only occur in the direct vicinity of the ALM. All differences in the wake flow therefore trace back to local changes near the rotor plane. In this way, the presented results are in agreement with the initial assumptions on the locality of compressibility. Furthermore, it is shown that even large relative changes in the dilation due to small ϵ only mildly affect the wake flow characteristics. From an ALM perspective this can be appreciated. Ultimately, it implies that the smearing width as such does not introduce significant ALM-specific compressibility-related effects on the flow field in addition to those known from incompressible frameworks [21, 44, 45].

Using the fully-coupled ALM compressibility can become an issue for the accurate computation of the rotor forces. More precisely, it can introduce deviations from the angle of attack as predicted by BEM theory. These deviations come in addition to those also present in incompressible frameworks near the root and tip. Regardless of the compressibility of the surrounding fluid, deviations from BEM theory are undesirable for the ALM. Discussions on compressibility in the context of ALM simulations as presented in [6] should thus be taken with due care. After all, changes in the wake flow field can be attributed to compressibility-related changes in the forces of the ALM and not necessarily compressibility effects in the flow. Eventually, additional correction models might be required to mitigate such deviations.

At last, following conclusions can be drawn regarding the the two main motivations of this study. The former was the comparison of (near-)incompressible to (Mach-matched) compressible wake flows. Bearing in mind that the latter corresponds to Ma_{pc} the observed differences can arguably be considered negligible. This even corresponds to the fully-coupled ALM cases which include the aforementioned changes in the blade forces. In agreement with the common practice we therefore conclude that compressibility can be neglected when simulating wind turbine wakes. The second motivation was the investigation of wake flows with artificially increased compressibility as commonly done in weakly compressible frameworks. As for the wake alone compression/expansion was consistently found to remain negligible even for the highest investigated Mach number. The blade-induced dilatation of the rotor, however, can reach magnitudes which locally exceed the non-negligible regime depending on the smearing width. Hence, it should be taken into account that this formally violates the underlying weakly-compressible assumption even though the impact on the wake remains reasonably small.

References

[1] Mehta D, van Zuijlen A, Koren B, Holierhoek J and Bijl H 2014 *J. Wind Eng. Ind. Aerodyn.* **133** 1 – 17
[2] Vermeer L, Sørensen J and Crespo A 2003 *Prog. Aerosp. Sci.* **39** 467 – 510
[3] Campobasso M S, Yan M, Drofelnik J, Piskopakis A and Caboni M 2014 *Proc. ASME Turbo Expo: Power for Land, Sea, and Air* V03BT46A010
[4] Sørensen N N, Bertagnolio F, Jost E and Lutz T 2018 *J. Phys. Conf. Ser.* **1037** 022003
[5] Glauert H 1928 *P. R, Soc. Lond. A-CONTA* **118** 113–119
[6] Yan C and Archer C L 2018 *Appl. Energ.* **212** 33 – 45
[7] Wood D 1997 *Renew. Energ.* **10** 11–17
[8] Bazilevs Y, Hsu M C, Kiendl J, Wüchner R and Bletzinger K U 2011 *Int. J. Numer. Meth. Fl.* **65** 236–253
[9] Cai X, Gu R, Pan P and Zhu J 2016 *Energy Conversion and Management* **112** 146–156
[10] Sørensen J N and Shen W Z 2002 *J. Fluids Eng.* **124** 393–399
[11] Chassaing P, Antonia R A, Anselmet F and Sarkar L J S 2002 *Variable Density Turbulence* (New York, USA: Springer)
[12] Sagaut P and Cambon C 2018 *Homogeneous Turbulence Dynamic* (Springer International Publishing)
[13] Donzis D A and Jagannathan S 2013 *J. Fluid. Mech.* **733** 221–244
[14] Bull J R and Jameson A 2015 *AIAA Journal* **53** 2750–2761
[15] Lenz S, Schönherr M, Geier M, Krafczyk M, Pasquali A, Christen A and Giometto M 2019 *J. Win. Eng. Ind. Aerod.* **189** 151 – 162
[16] Löhner R 2019 *Int. J. Comput. Fluid. D.* **33** 87–97
[17] Deiterding R and Wood S L 2016 *J. Phys.: Conf. Series* **753** 082005
[18] Rullaud S, Blondel F and Cathelain M 2018 *J. Phys.: Conf. Series* **1037** 022023

[19] Asmuth H, Olivares-Espinosa H, Nilsson K and Ivanell S 2019 *J. Phys. Conf. Ser.* **1256** 012022
[20] Asmuth H, Olivares-Espinosa H and Ivanell S 2019 *Wind Energ. Sci. Discuss.* **2019** 1–33
[21] Meyer Forsting A R, Pirrung G R and Ramos-García N 2019 *Wind Energ. Sci.* **4** 369–383
[22] Elie B, Oger G, Guillerm P E and Alessandrini B 2017 *Renew. Energ.* **108** 336 – 354
[23] Elie B, Oger G and Le Touzé D 2019 *Proc. ASME 2019 2nd International Offshore Wind Technical Conference*
[24] Krüger T, Kusumaatmaja H, Kuzmin A, Shardt O, Silva G and Viggen E M 2016 *The Lattice Boltzmann Method - Principles and Practice* (Heidelberg, Germany: Springer)
[25] Bhatnagar P, Gross E and Krook M 1954 *Phys. Rev.* **94**(3) 511–525
[26] Coreixas C, Chopard B and Latt J 2019 *Phys. Rev. E* **100**(3) 033305
[27] Geier M, Schönherr M, Pasquali A and Krafczyk M 2015 *Comput. Math. Appl.* **70** 507–547
[28] Lallemand P and Luo L S 2000 *Phys. Rev. E* **61**(6) 6546–6562
[29] Geier M, Pasquali A and Schönherr M 2017 *J. Comput. Phys.* **348** 862–888
[30] Dubois F 2008 *Comp. Math. Appl.* **55** 1441 – 1449
[31] Marié S, Ricot D and Sagaut P 2009 *J. Comput. Phys.* **228** 1056 – 1070
[32] Brès G, Pérot F and Freed D 2017 *Proc. 15th AIAA/CEAS Aeroacoustics Conference*
[33] Dellar P J 2014 *J. Comput. Phys.* **259** 270 – 283
[34] Janßen C F, Mierke D, Überrück M, Gralher S and Rung T 2015 *Computation* **3** 354
[35] Gehrke M, Janßen C and Rung T 2017 *Comput. Fluids* **156** 247–263
[36] Gehrke M, Banari A and Rung T 2020 *Notes on Numerical Fluid Mechanics and Multidisciplinary Design. Progress in Hybrid RANS-LES Modelling* **143** 3–18
[37] Jonkman J, Butterfield S, Musial W and Scott G 2009 Definition of a 5-MW reference wind turbine for offshore system development Tech. Rep. NREL/TP-500-38060 NREL
[38] Mann J 1998 *Probabilist. Eng. Mech.* **13** 269 – 282
[39] Malaspinas O and Sagaut P 2012 *J. Fluid. Mech.* **700** 514–542
[40] Pasquali A, Geier M and Krafczyk M 2017 *Comput. Math. Appl.* **79** 195–212
[41] Lee K, Girimaji S S and Kerimo J 2009 *J. Turbul.* **10** N9
[42] Suman S and Girimaji S S 2010 *J.Turbul.* **11** N2
[43] Jha P K and Schmitz S 2018 *J. Fluid Mech.* **834**
[44] Martínez-Tossas L A and Meneveau C 2019 *J. Fluid Mech.* **863** 269–292
[45] Martínez-Tossas L A, Churchfield M J and Meneveau C 2017 *Wind Energy* **20** 1083–1096